

Ultralong organic room-temperature phosphorescence modulated by balancing intramolecular charge transfer and localized excitation character of excited states



Tengyue Wang, Xuepu Wang, Qianqian Yan ^{**}, Kaka Zhang ^{*}

State Key Laboratory of Organometallic Chemistry, Key Laboratory of Synthetic and Self-Assembly Chemistry for Organic Functional Molecules, Shanghai Institute of Organic Chemistry, University of Chinese Academy of Sciences, Chinese Academy of Sciences, 345 Lingling Road, Shanghai, 200032, People's Republic of China

ARTICLE INFO

Keywords:

Afterglow
Localized excitation
Intramolecular charge transfer
Phosphorescence

ABSTRACT

Long emission lifetime is the defining character of organic room-temperature phosphorescence (RTP) and afterglow materials. In the absence of heavy atom effect, organic localized excitation (LE) systems show small phosphorescence rates and exhibit potential to form long-lived phosphorescence materials. However, such LE systems usually have limited population of T_1 states because of large singlet-triplet splitting energy (ΔE_{ST} , around 1 eV). Here we report ultralong RTP by balancing intramolecular charge transfer and localized excitation character of excited states. Aromatic functional groups of moderate electron-donating strength are selected to build difluoroboron β -diketonate (BF_2bdk) systems with moderate intramolecular charge transfer (ICT) character in their S_1 states. Such molecular design gives rise to ΔE_{ST} around 0.5 eV and is enough to populate BF_2bdk 's T_1 states. Significantly, the resultant BF_2bdk 's T_1 states exhibit 85–90% 3LE character and display long phosphorescence lifetimes up to 1.38 s upon doping under ambient conditions. This study shows that simple design of organic system can also lead to high-performance RTP materials and provide an insight into the fundamental photophysics of organic triplet system.

1. Introduction

The long-lived excited state nature constitutes one of the defining features of room-temperature phosphorescence (RTP) and organic afterglow materials [1–8]. These materials offer advantage of eliminating the interference from background fluorescence, making them well-suited for applications in optical sensing, biological imaging and data encryption [9–12]. In conventional organic molecular system, the spin-forbidden transitions between states of differing multiplicities lead to small rate constants of intersystem crossing (k_{ISC}) from singlet excited state to triplet excited state and low quantum yields of intersystem crossing (Φ_{ISC}), so the population of organic triplets is less favored [13–16]. Even when it is feasible to populate the triplet excited state, due to the relatively modest rate constant of phosphorescence decay (k_P) and the comparatively substantial rate constant of nonradiative deactivation (k_{nr}) and quenching process (k_q) of organic triplets at room temperature, it remains a formidable task to attain organic materials with high phosphorescence quantum yields (Φ_P) at room temperature

[17–25].

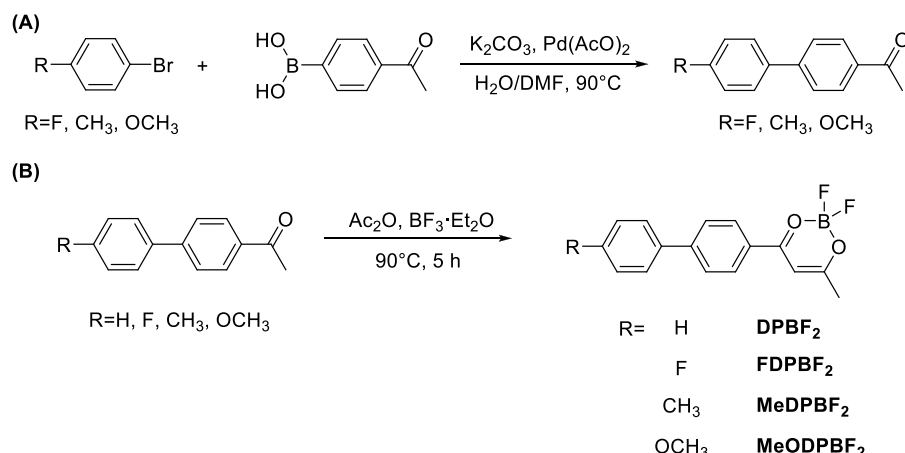
In the last decades, heavy-atom effects and $n-\pi^*$ transitions have been widely applied to accelerate intersystem crossing and phosphorescence decay, consequently enhancing the efficiency of organic afterglow [3, 17, 18]. However, heavy-atom effects often give rise to a marked increase in phosphorescence decay rates, thus diminishing phosphorescence lifetimes. Besides, the involvement of $n-\pi^*$ transitions in organic T_1 states also accelerates phosphorescence decay and decreases phosphorescence lifetimes [3, 17, 18]. For instance, in benzophenone systems, T_1 states of $^3n-\pi^*$ transition character exhibit phosphorescence decay rates of approximately 10^3 s⁻¹ and phosphorescence lifetimes of approximately 1 ms [3, 17, 18]. Notably, in these organic systems with heavy atom effects and $n-\pi^*$ transitions, intersystem crossing rates and phosphorescence rates are inextricably linked; they rise and fall together. The consequence of this correlation is that high afterglow efficiency conflicts with long afterglow lifetimes in organic systems, a recurrent quandary in the field.

In view of the design strategies that can exclusively augment k_{ISC}

* Corresponding author.

** Corresponding author.

E-mail addresses: yanqianqian@sioc.ac.cn (Q. Yan), zhangkaka@sioc.ac.cn (K. Zhang).



Scheme 1. Synthesis routes of DPBF₂ and DPBF₂ derivatives.

without significantly affecting k_p , we reason that, by effectively suppressing k_{nr} and k_q , organic systems with enhanced k_{ISC} and diminished k_p would exhibit highly-efficient and long-lived RTP properties. The two-component design strategy, wherein a second component modulates the excited state property of luminescent component (the first component), has demonstrated remarkable efficacy in fashioning high-performance afterglow materials under ambient conditions [21, 26–38]. For instance, organic matrices (the second component) in crystalline or glassy states are able to constrain luminescent component's intramolecular motions, thereby minimizing k_{nr} of luminescent component's triplets [21]. In two-component systems composed of electron-donating molecules and electron-accepting molecules, photo-induced intermolecular charge transfer, subsequent charge separation and slow charge recombination have paved the way for developing afterglow materials with hour-long duration [2, 34, 39–43]. Organic matrices with suitable positioned T₁ levels have also been documented to mediate luminescent component's singlet-to-triplet intersystem crossing [44–46]. Our recent studies have unveiled the capacity of organic matrices with dipole moments to perturb luminescent component's S₁ states through dipole-dipole interactions, thereby reducing singlet-triplet splitting energy (ΔE_{ST}) and enhancing intersystem crossing [47–51].

The advantages of the two-component design strategy are multifaceted: (1) it affords flexibility in the selection of both components with less synthetic works; (2) by holding one component constant and systematically adjusting the other, comprehensive insight into the underlying photophysics are obtained, which guide the fabrication of high-performance afterglow materials; (3) when external physical, chemical or biological stimuli perturb the properties of either component or their interactions, stimuli-responsive afterglow materials exhibiting intriguing photophysical behaviors would come into fruition.

Adhering to the energy gap law, the reduction of ΔE_{ST} can lead to the increase of k_{ISC} values. Based on this, the combination of charge transfer technology and dopant-matrix strategy to reduce ΔE_{ST} is explored. The critical design factors are listed as follows: (1) The selection of organic luminescent compounds with intramolecular charge transfer (ICT) characteristics is important. Owing to the HOMO-LUMO separation inherent to CT systems, the ΔE_{ST} values of organic CT systems (typically around 0.5 eV or less) are notably smaller than those in organic localized excitation (LE) systems (often exceeding 0.5 eV and even 1.0 eV) [31, 51, 52]. The exchange energy of two unpaired electrons at excited states governs the ΔE_{ST} value; the HOMO-LUMO separation in organic CT system effectively reduces ΔE_{ST} value. (2) The S₁ states of organic CT molecules exhibit substantial dipole moments. Dipole-dipole interactions between the S₁ states and organic matrices, such as ketones, esters and even simple aromatics, have demonstrated the capacity to

diminish S₁ levels while having insignificant impact on T₁ levels, thereby narrowing ΔE_{ST} and enhancing k_{ISC} [49–51, 53, 54]. This dipole effect has been corroborated through ultrafast time-resolved photoluminescence study recently. Theoretical calculation has shown that only a decrease of ΔE_{ST} by 0.05 eV can result in the acceleration of k_{ISC} by around 10 times. (3) Unlike heavy atom effect and $n-\pi^*$ transition that simultaneously increase k_{ISC} and k_p , the strategies outlined in (1) and (2) exert a limited effect on k_p . When the organic CT systems exhibit small k_p values, the application of two-component dopant-matrix strategy becomes necessary to inhibit k_{nr} and k_q of the T₁ states by employing rigid organic matrices for fabricating afterglow materials with long phosphorescence lifetimes (τ_p).

There are limited examples of CT systems in the reported studies exhibiting ultralong phosphorescence lifetimes, for example, longer than 1.0 s and even 1.5 s [55–57]. It has been found that in these CT systems, their T₁ states are also mainly of CT characters like their S₁ states [55–57]. Based on the fundamental property that k_p align in the order of ${}^3\text{LE} < {}^3\text{ICT} < {}^3n-\pi^*$ transition, the augmentation of ${}^3\text{LE}$ characters in organic T₁ states is the key to achieve long phosphorescence lifetimes under ambient conditions [3, 56–58]. Recent advancements, facilitated by the facile synthesis of difluoroboron β -diketonate (BF₂bdk) compounds through our cascade reactions, have yielded an array of two-component BF₂bdk-matrix afterglow systems that exhibit intriguing photophysical property and high performance [26, 56, 59–61]. Most BF₂bdk compounds show typical CT characters from electron-donating aromatic groups to electron-deficient dioxaborine groups. BF₂bdk systems show LUMO levels of approximately –2.6 eV, while their HOMO levels can be controlled by electron-donating aromatic groups. Here we design a series of BF₂bdk with adjustable electron-donating strengths of aromatic groups (Scheme 1). When the electron-donating strength is moderate, TD-DFT calculation reveals that the resultant BF₂bdk has ${}^3\text{LE}$ character of 85%–90% in its T₁ state. Consequently, phosphorescence lifetime longer than 1.0 s has been achieved by doping the BF₂bdk into suitable organic matrix. Further, after deuteration of the BF₂bdk to reduce intramolecular motion (such as C–H vibration) of its T₁ state, phosphorescence lifetime exceeds 1.6 s.

2. Experimental section

2.1. Synthesis of BF₂bdk compounds

2.1.1. Synthesis of DPBF₂

Into a round bottom flask were added 4-acetyl biphenyl (392 mg, 1.0 mmol), acetic anhydride (6.00 mL) and boron trifluoride diethyl etherate (1.2 mL, 9.5 mmol). The reaction mixture was heated at 80 °C for 5 h. After cooling to room temperature, the reaction mixture was

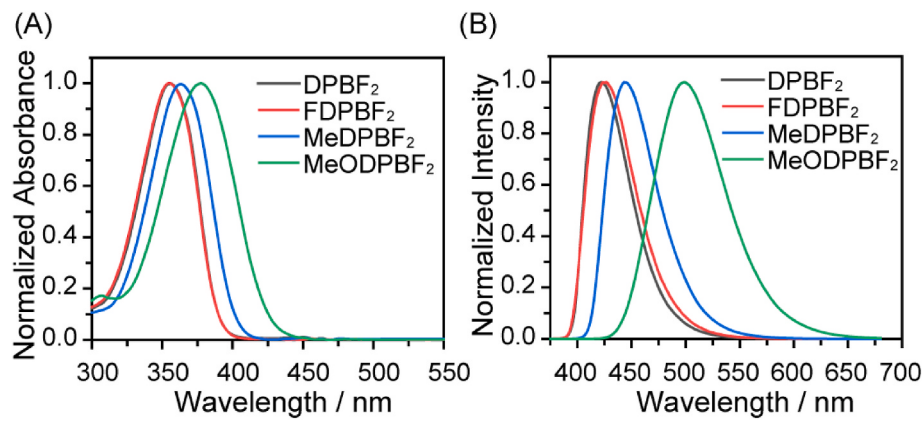


Fig. 1. (A) UV-vis spectra and (B) steady-state emission spectra of the BF₂bdk compounds in dichloromethane solution at room temperature.

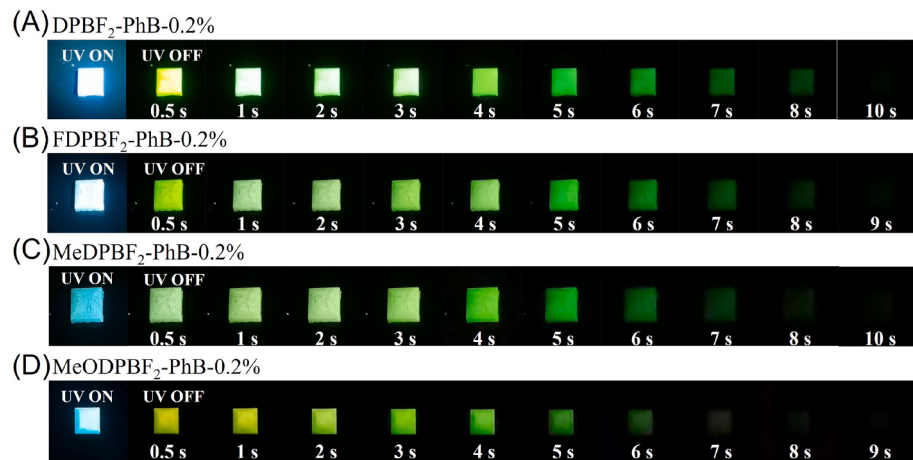


Fig. 2. Photographs of (A) DPBF₂-PhB-0.2%, (B) FDPBF₂-PhB-0.2%, (C) MeDPBF₂-PhB-0.2%, and (D) MeODPBF₂-PhB-0.2% under 365 nm UV light and after removal of the UV light at room temperature.

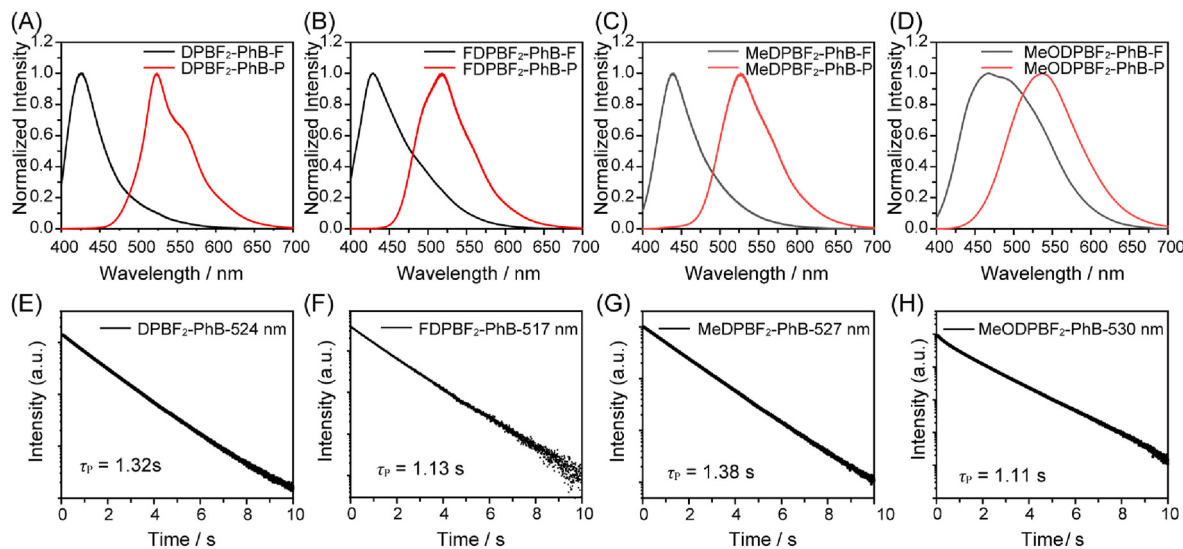


Fig. 3. Room-temperature steady-state (black line) and delayed emission spectra (red line) of (A) DPBF₂-PhB-0.2%, (B) FDPBF₂-PhB-0.2%, (C) MeDPBF₂-PhB-0.2%, and (D) MeODPBF₂-PhB-0.2% materials. Room-temperature phosphorescence decay of (E) DPBF₂-PhB-0.2%, (F) FDPBF₂-PhB-0.2%, (G) MeDPBF₂-PhB-0.2%, and (H) MeODPBF₂-PhB-0.2% materials.

Table 1
Photophysical properties of BF₂bdk-PhB-0.2% melt-cast samples.

Sample	λ_F (nm)	λ_P (nm)	ΔE_{ST} (eV)	τ_p (s)	PLQY (%)
DPBF ₂ -PhB-0.2%	427	524	0.54	1.32	34.2
FDPBF ₂ -PhB-0.2%	428	518	0.50	1.13	34.6
MeDPBF ₂ -PhB-0.2%	438	527	0.48	1.38	60.0
MeODPBF ₂ -PhB-0.2%	460	531	0.36	1.11	51.9

extracted with dichloromethane and deionized water. The organic phase was collected and dried over anhydrous sodium sulfate, condensed by rotary evaporation, and then purified by column chromatography over silica gel using the petroleum ether/dichloromethane (1.5/1, v/v) as eluent to give 471.9 mg pale yellow solids with an isolation yield of 82.5%. The obtained DPBF₂ was isolated as crystalline products in spectroscopic grade dichloromethane/n-hexane. ¹H NMR (400 MHz, Chloroform-d, relative to Me₄Si/ppm) δ 8.15–8.12 (m, 2H), 7.77–7.74 (m, 2H), 7.66–7.63 (m, 2H), 7.51–7.46 (m, 2H), 7.46–7.42 (m, 1H), 6.61 (s, 1H), 2.43 (s, 3H). ¹³C NMR (126 MHz, Chloroform-d) δ 192.25, 182.49, 148.39, 139.20, 129.91, 129.80, 129.27, 129.07, 127.84, 127.46, 97.17, 24.91. ¹⁹F NMR (376 MHz, Chloroform-d) δ –138.82 (19.8%), –138.88 (80.2%). HRMS (positive ESI) *m/z* found (calcd for C₁₆H₁₃BF₂O₂+Na⁺): 309.0869 (309.0872).

2.1.2. Synthesis of FDPBF₂

Into a round bottom flask were added 4-fluorobenzeneboronic acid (139.9 mg, 1.0 mmol), 4'-bromoacetophenone (298.56 mg, 1.5 mmol), K₂CO₃ (138.2 mg, 3 mmol), (CH₃COO)₂Pd (2.3 mg, 0.01 mmol), DMF (8 mL) and water (2 mL). The reaction mixture was heated at 90 °C for 6 h. After cooling to room temperature, excess water was added to the

reaction mixture, leading to the precipitation of crude product. After filtration and washing by water, DMF was removed. The crude product was dissolved in dichloromethane, dried with anhydrous sodium sulfate. After the filtration, the product was concentrated by rotary evaporation. The crude product was purified by column chromatography over silica gel using petroleum ether/dichloromethane (3:1) to give white solids 4'-fluoro-4-acetyl biphenyl (175.5 mg, yield 81.9%). Then following the same procedure with the synthesis of DPBF₂, the yellow solid FDPBF₂ was obtained (177.8 mg, 71.4%). ¹H NMR (400 MHz, Chloroform-d, relative to Me₄Si/ppm) δ 8.15–8.12 (m, 2H), 7.73–7.65 (m, 2H), 7.65–7.60 (m, 2H), 7.21–7.19 (m, 2H), 6.61 (s, 1H), 2.44 (s, 3H). ¹³C NMR (126 MHz, Chloroform-d) δ 192.42, 182.34, 164.48, 162.50, 147.24, 135.34, 135.31, 129.92, 129.84, 129.25, 129.18, 127.65, 116.37, 116.20, 97.49, 24.91. ¹⁹F NMR (376 MHz, Chloroform-d) δ –112.55 (dq, *J* = 8.9, 4.5 Hz), –138.71, –138.77. HRMS (positive ESI) *m/z* found (calcd for C₁₆H₁₂BF₃O₂+K⁺): 343.0514 (343.0517).

2.1.3. Synthesis of MeDPBF₂

By replacing 4-fluorobenzeneboronic acid with 4-

Table 2

Calculated LE and CT contributions to the lowest-lying singlet (S₁) and triplet (T₁) excited states of DPBF₂ and DPBF₂ derivatives.

Molecule	¹ CT	¹ LE	³ CT	³ LE
DPBF ₂	42.74%	57.26%	8.66%	91.34%
FDPBF ₂	45.44%	54.56%	9.58%	90.42%
MeDPBF ₂	47.57%	52.44%	13.28%	86.72%
MeODPBF ₂	53.77%	46.23%	22.46%	77.54%

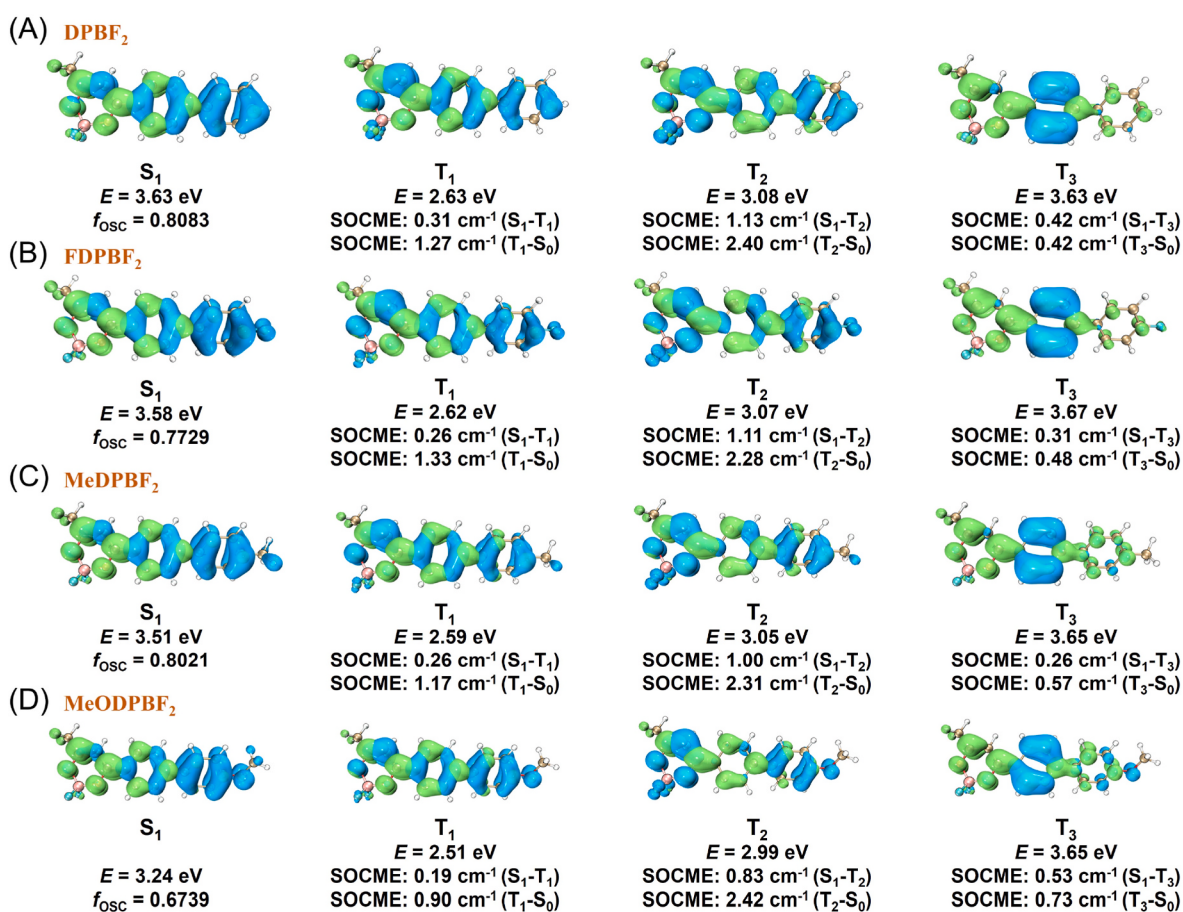


Fig. 4. Iso-surface maps of the electron-hole density difference of BF₂bdk's S₁ and T_n states calculated in Gaussian 16 by TD-DFT/B3LYP/6-31G (d,p), where blue and green iso-surfaces correspond to hole and electron distributions, respectively. SOCME values calculated on ORCA 5.0.4 by TD-DFT/B3LYP/def2-TZVP(-f).

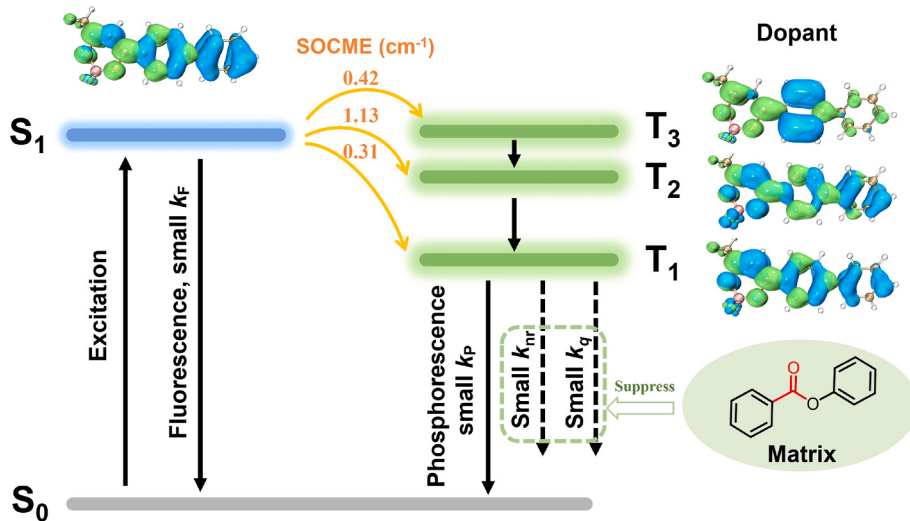


Fig. 5. Proposed RTP mechanism of the BF_2bdk -PhB afterglow system.

methylphenylboronic acid (135.96 mg, 1.0 mmol), MeDPBF₂ as a yellow solid (167.9 mg, yield 69.4%) was obtained through the same experimental steps as the synthesis of FDPBF₂. ¹H NMR (400 MHz, Chloroform-*d*, relative to Me₄Si/ppm) δ 8.13–8.10 (m, 2H), 7.74–7.72 (m, 2H), 7.56–7.54 (m, 2H), 7.31–7.29 (d, *J* = 7.9 Hz, 2H), 6.59 (s, 1H), 2.42 (s, 6H). ¹³C NMR (126 MHz, Chloroform-*d*) δ 192.03, 182.47, 148.33, 139.26, 136.22, 129.99, 129.81, 129.54, 127.50, 127.28, 97.40, 24.85, 21.36. ¹⁹F NMR (376 MHz, Chloroform-*d*) δ -138.88, -138.95. HRMS (positive ESI) *m/z* found (calcd for C₁₇H₁₅BF₂O₂+K⁺): 339.0764 (339.0768).

2.1.4. Synthesis of MeODPBF₂

By replacing 4-fluorobenzeneboronic acid with 4-methoxyphenylboronic acid (152 mg, 1.0 mmol), MeODPBF₂ as a yellow solid (155.09 mg, yield 65.5%) was obtained through the same experimental steps as the synthesis of FDPBF₂. ¹H NMR (400 MHz, Chloroform-*d*, relative to Me₄Si/ppm) δ 8.12–8.10 (m, 2H), 7.73–7.71 (m, 2H), 7.63–7.61 (m, 2H), 7.03–7.01 (m, 2H), 6.59 (s, 1H), 3.88 (s, 3H), 2.43 (d, *J* = 0.9 Hz, 3H). ¹³C NMR (126 MHz, Chloroform-*d*) δ 191.80, 182.45, 160.62, 147.98, 131.45, 129.87, 129.14, 128.66, 127.11, 114.71, 97.31, 55.56, 24.84. ¹⁹F NMR (376 MHz, Chloroform-*d*) δ -125.73, -125.79. HRMS (positive ESI) *m/z* found (calcd for C₁₇H₁₅BF₂O₃+K⁺): 355.0716 (355.0717).

2.2. Preparation of afterglow materials by doping BF_2bdk into organic matrices

For the preparation of two-component RTP systems, 100 mg phenyl benzoate (PhB) and 200 μL solution of DPBF₂ in dichloromethane (1.0 mg/mL) were added into an agate mortar (diameter = 5 cm). After grinding and solvent evaporating, DPBF₂-PhB-0.2% powders were heated to 75 °C to give a molten mixture. After standing at room temperature for tens of minutes, DPBF₂-PhB-0.2% afterglow materials were obtained. FDPBF₂-PhB-0.2%, MeDPBF₂-PhB-0.2% and MeODPBF₂-PhB-0.2% melt-cast samples were prepared through similar processes.

2.3. TD-DFT calculations

TD-DFT calculations were performed to investigate the photo-physical properties of BF_2bdk compounds in the solid state. Since the vibrations and rotations of the compounds being suppressed in the matrix, the optimized ground state geometry of BF_2bdk compounds was applied for TD-DFT calculations. The ground-state geometry of DPBF₂ and DPBF₂ derivatives were optimized by a DFT calculation using B3LYP

functional and 6-31G (d, p) basis set on Gaussian 16 program (Revision A.03) [62–64]. The singlet excited states and triplet excited states were calculated on Gaussian 16 program (Revision A.03) with TD-B3LYP functional and 6-31G (d, p) functional [62–64]. The singlet and triplet states, along with the spin-orbit coupling (SOC), were computed using ORCA 5.0.4 with the B3LYP general function and def2-TZVP basis set [65]. All isosurface maps to show the electron distribution and electronic transitions were rendered by Visual Molecular Dynamics (VMD) software based on the exported files from Multiwfn [66–68]. To calculate local-excitation (LE) and charge-transfer (CT) contributions to the lowest-lying singlet (S_1) and triplet (T_1) excited states of DPBF₂ derivatives, natural transition orbital (NTO) analyses were conducted on Gaussian 16 program (Revision A.03), and calculated fragment contributions by Hirshfeld method on Multiwfn 3.8 (dev) [52,62,66,69].

3. Results and discussion

A series of BF_2bdk compounds DPBF₂, FDPBF₂, MeDPBF₂ and MeOBF₂ with different electron-withdrawing or electron-donating substituents were designed and synthesized by one or two steps (Scheme 1). First, the 4-acetyl biphenyl derivatives were obtained via Suzuki coupling reaction between 4-bromobenzene derivatives and 4-acetylphenylboronic acid, then followed by a cascade reaction with the addition of acetic anhydride and boron trifluoride diethyl etherate [26, 59–61]. The pure BF_2bdk compounds were obtained after column chromatography and subsequent three-cycle recrystallization. The structures of BF_2bdk compounds were carefully characterized by ¹H NMR, ¹³C{¹H} NMR, ¹⁹F{¹H} NMR, HRMS. Single crystals of DPBF₂ and MeDPBF₂ were grown from slow evaporation in dichloromethane and *n*-hexane solution. The high purity of compounds was further confirmed by HPLC.

UV-vis spectrum of DPBF₂ compound in dichloromethane solution shows an intense absorption band from 275 to 400 nm centered at 355 nm with molar absorption constant of $5.88 \times 10^4 \text{ M}^{-1}\text{cm}^{-1}$ (Fig. 1A), which can be assigned as ICT transition from the biphenyl moieties (electron donor) to boron (III) diketonate moieties (electron acceptor). The solution exhibits intense blue emission and show an emission band from 385 to 500 nm with maxima at 425 nm in the steady-state fluorescence spectrum (Fig. 1B). Comparing to DPBF₂, the absorption spectra of FDPBF₂, MeDPBF₂ and MeODPBF₂ in dichloromethane solution also show an intense absorption band from 275 nm to 450 nm and centered at 355 nm, 363 nm, and 378 nm, respectively. The absorption maxima of MeDPBF₂ and MeODPBF₂ compounds with electron-donating substituent show significantly red shift. Their emission spectra show

bands ranging from 385 to 650 nm with red-shift maxima at 422, 443, and 498 nm, respectively. The photophysical properties were summarized in Table S1. The absorption and emission spectra of DPBF₂ and the derivatives in different solvents show a red shift when the solvent polarity is increasing (Fig. S1 and Fig. S2), suggesting the ICT characteristics of the S₁ state of DPBF₂ molecules.

DPBF₂ powders exhibit bright emission under 365 nm UV lamp but no afterglow was observed after ceasing the light source (Fig. S3). Here, dopant-matrix strategy was employed to fabricate room-temperature phosphorescence materials, where a second component is used to control the properties of triplet excited state. The selection of organic matrices is very important. In our previous studies, phenyl benzoate (PhB) has been reported that it shows good performance as the matrix [26,56,57,59–61,70,71]. First, organic matrices with dipole moments interact with BF₂bdk excited state via dipole-dipole interactions and reduce S₁ levels of BF₂bdk, with decreasing of ΔE_{ST} value and enhancement of ISC [47–51]. Second, PhB has much lower HOMO energy level of –6.96 eV and higher LUMO energy level of –1.79 eV than the BF₂bdk dopant, which precludes the formation of intermolecular charge transfer complexes with the BF₂bdk dopants. Third, PhB possesses a high T₁ level (3.53 eV) calculated by TD-DFT, which is higher than BF₂bdk's. It prevents quenching or reduction in RTP performance by energy transfer from the dopants' T₁ to PhB's T₁ triplet excited state [71]. Forth, crystalline PhB can suppress nonradiative decay and oxygen quenching of T₁ states. Additionally, PhB have a low melting point of 68–70 °C, which allows the materials to be easily constructed into desired shapes with the aid of silicone molds. PhB powders show negligible absorption above 365 nm and show no afterglow at room temperature. When doping DPBF₂ into PhB at 0.2 wt% concentration via melt-cast strategy, the obtained DPBF₂-PhB-0.2% show significant afterglow properties under ambient conditions (Fig. 2A). It shows intense blue emission under 365 nm UV lamp and exhibit bright green afterglow with a duration of 10 s. FDPBF₂-PhB-0.2%, MeDPBF₂-PhB-0.2% and MeODPBF₂-PhB-0.2% RTP materials were also prepared following the similar procedures, exhibiting ultralong green afterglow emission with the duration of 9 s, 10 s, and 9 s, respectively (Fig. 2B–D).

Next, the photophysical properties of dopant-matrix systems were investigated. The steady-state emission spectrum of DPBF₂-PhB-0.2% shows an emission band from 400 to 600 nm with a maximum emission peak at 427 nm. The delayed emission spectrum shows an emission band in the range of 450–700 nm, with emission maxima at 524 nm and a shoulder peak at 556 nm (Fig. 3A). The ΔE_{ST} value, which is estimated from the fluorescence and phosphorescence maxima, is 0.54 eV. The delayed emission spectra at 77 K were also measured (Figs. S4 and S5), exhibiting an emission band from 400 nm to 600 nm, which locates in the same region as the room-temperature delayed emission band, suggesting that this band originates from phosphorescence. The phosphorescence decay of DPBF₂-PhB-0.2% samples follow exponential decay, with an ultralong τ_p of 1.32 s at room temperature (Fig. 3E). Photoluminescence quantum yields (PLQYs) of DPBF₂-PhB-0.2% samples have been measured to be 34.2%. Further, it has been reported that the deuteration of luminescent molecule can enhance the RTP emission, resulting from the reduction of the intramolecular motions and non-radiative decay of triplet states since the vibration of C–D bonds is much weaker than C–H bonds [53,72,73]. The deuterated DPBF₂ (*d*-DPBF₂) were prepared following the reported literature [53]. When *d*-DPBF₂ were doped into PhB at 0.2 wt% concentration, the obtained *d*-DPBF₂-PhB-0.2% exhibit very intense afterglow as expected. Their steady state spectra and delayed emission spectra display a similar band with DPBF₂-PhB-0.2% (Fig. S6). However, phosphorescence lifetime of *d*-DPBF₂-PhB-0.2% is up to 1.61 s. Based on the above results, we reason that the phosphorescence originated from the BF₂bdk's T₁ states in PhB matrices.

Similarly, the steady-state emission spectra of FDPBF₂-PhB-0.2%, MeDPBF₂-PhB-0.2% and MeODPBF₂-PhB-0.2% exhibit emission bands

ranging from 400 nm to 600 nm with emission maxima at 428 nm, 438 nm, and 460 nm, respectively (Fig. 3B–D). Their delayed emission spectra (1 ms delay) show emission bands in the range of 450–700 nm with slightly red-shift emission maxima at 518 nm, 527 nm, and 531 nm, respectively (Fig. 3B–D). It is worth to note that the ΔE_{ST} value were estimated to be 0.50 eV, 0.48 eV, and 0.36 eV, respectively. Interestingly, from their excited state decay profiles, it is found that the afterglow emission lifetime of FDPBF₂-PhB-0.2% and MeODPBF₂-PhB-0.2%, which containing electron-withdrawing or stronger electron-donating substitute, was calculated to be 1.13 s and 1.11 s, respectively (Fig. 3F–H). They are shorter than τ_p of DPBF₂-PhB-0.2%. The PLQYs were determined to be 34.6% and 52.0% at room temperature. However, MeDPBF₂-PhB-0.2% samples, which containing moderate electron-donating substitute, possess longer τ_p than DPBF₂-PhB-0.2%. The τ_p was calculated up to 1.38 s and PLQY can be increased to 60% (Fig. 3G and Table 1).

To further understand the photophysical behaviors of dopant-matrix systems, theoretical studies on those systems were performed. The time-dependent density functional theory (TD-DFT) calculations clearly indicate that the S₁ state of DPBF₂ and its derivatives possesses a large portion of CT characters (Fig. 4), consistent with the results in UV-vis spectra. The ΔE_{ST} in S₁-T₂ and S₁-T₃ ISC channels is smaller than the S₁-T₁ ISC channel. The spin-orbit coupling matrix elements (SOCME) values of DPBF₂, FDPBF₂, MeDPBF₂ and MeODPBF₂ in S₁-T₂ ISC channel reach to 1.13 cm^{–1}, 1.11 cm^{–1}, 1.00 cm^{–1}, and 0.83 cm^{–1}, respectively, larger than in S₁-T₁ ISC channel. Therefore, BF₂bdk's ISC can be mediated by S₁-T₂ and S₁-T₃ ISC channels. The natural transition orbital (NTO) of BF₂bdk compounds were evaluated (Fig. S26 and Fig. S27). The holes distribute on biphenyl and its substitute, while the electrons are mainly spread over difluoroboron-β-diketonate moiety. The LE and CT contributions to both the S₁ and T₁ states of BF₂bdk compounds were calculated, as shown in Table 2. It is interesting to find that its T₁ state mainly exhibits LE character. The participation of ³LE components can contribute to the reduction of k_p since ³LE states have a smaller k_p compared to ³CT and ³n-π* states. The T₁ state of BF₂bdk compounds exhibiting CT plus LE characters results in a small k_p , which potentially enables the formation of RTP emitters with long τ_p . When the electron-donating strength is moderate, the resultant MeDPBF₂ has ³LE character of 86.72% in its T₁ state with small ΔE_{S1-T2} and relatively high SOCME of S₁ to T₁. However, the T₁ states of MeODPBF₂ with stronger donating group display elevated CT qualities, leading to shorter τ_p lifetimes, limiting the production of extremely prolonged organic RTP. Hence, excessive CT characters need to be prevented to accomplish ultralong RTP under ambient temperatures. In addition, the crystalline PhB matrices prevent non-radiative decay and oxygen quenching of the BF₂bdk triplets, resulting in a high-performance BF₂bdk-PhB organic afterglow materials at ambient conditions (Fig. 5).

4. Conclusion

In summary, we have designed a series of BF₂bdk phosphors with adjustable electron-donating strengths of aromatic groups. High performance RTP materials were fabricated based on two-component strategy and balancing of CT and LE contributions in the excited states of BF₂bdk compounds. When MeDPBF₂ possessing moderate electron-donating group were doped in PhB matrix, the obtained RTP material MeDPBF₂-PhB-0.2% have a long τ_p up to 1.38 s and high PLQY of 60.0%. Theoretical calculations of the system show that it is most suitable when the ³LE character of the material reaches 85–90% to achieve ultralong phosphorescence. This work expands the scope of organic RTP materials and provides a new molecular design method for obtaining efficient RTP materials.

CRediT authorship contribution statement

Tengyue Wang: Writing – original draft, Formal analysis, Data

curation. **Xuepu Wang:** Formal analysis, Data curation. **Qianqian Yan:** Writing – review & editing, Supervision. **Kaka Zhang:** Writing – review & editing, Supervision, Project administration, Methodology, Funding acquisition.

Declaration of competing interest

The authors declare that they have no known competing financial interests or personal relationships that could have appeared to influence the work reported in this paper.

Data availability

Data will be made available on request.

Acknowledgements

We thank the financial supports from National Natural Science Foundation of China (22175194), Shanghai Scientific and Technological Innovation Project (20QA1411600, 20ZR1469200), Hundred Talents Program from Shanghai Institute of Organic Chemistry (Y121078), Pioneer Hundred Talents Program of Chinese Academy of Sciences (E320021), and Ningbo Natural Science Foundation (2023J243). We thank the staff at BL17B1 beamline of the National Facility for Protein Science in Shanghai (NFPS), Shanghai Advanced Research Institute, CAS, for providing technical support in X-ray diffraction data collection and analysis.

Appendix A. Supplementary data

Supplementary data to this article can be found online at <https://doi.org/10.1016/j.dyepig.2024.112024>.

References

- [1] Yam VW-W, Au VK-M, Leung SY-L. Light-emitting self-assembled materials based on d⁸ and d¹⁰ transition metal complexes. *Chem Rev* 2015;115:7589–728. <https://doi.org/10.1021/acs.chemrev.5b00074>.
- [2] Kabe R, Adachi C. Organic long persistent luminescence. *Nature* 2017;550:384–7. <https://doi.org/10.1038/nature24010>.
- [3] Zhao W, He Z, Tang BZ. Room-temperature phosphorescence from organic aggregates. *Nat Rev Mater* 2020;5:869–85. <https://doi.org/10.1038/s41578-020-0223-z>.
- [4] Gan N, Shi H, An Z, Huang W. Recent advances in polymer-based metal-free room-temperature phosphorescent materials. *Adv Funct Mater* 2018;28:1802657. <https://doi.org/10.1002/adfm.201802657>.
- [5] Ma X, Wang J, Tian H. Assembling-induced emission: an efficient approach for amorphous metal-free organic emitting materials with room-temperature phosphorescence. *Acc Chem Res* 2019;52:738–48. <https://doi.org/10.1021/acs.accounts.8b00620>.
- [6] Hirata S. Recent advances in materials with room-temperature phosphorescence: photophysics for triplet exciton stabilization. *Adv Opt Mater* 2017;5:1700116. <https://doi.org/10.1002/adom.201700116>.
- [7] Kenry, Chen C, Liu B. Enhancing the performance of pure organic room-temperature phosphorescent luminophores. *Nat Commun* 2019;10:2111. <https://doi.org/10.1038/s41467-019-10033-2>.
- [8] Li Q, Li Z. Molecular packing: another key point for the performance of organic and polymeric optoelectronic materials. *Acc Chem Res* 2020;53:962–73. <https://doi.org/10.1021/acs.accounts.0c00060>.
- [9] Wang G, Li J, Li X, Wang X, Sun Y, Liu J, et al. Two-component design strategy: TADF-Type organic afterglow for time-gated chemodosimeters. *Chem Eng J* 2022;431:134197. <https://doi.org/10.1016/j.cej.2021.134197>.
- [10] Yao H, Zhang Y, Wang G, Li J, Huang J, Wang X, et al. TADF-type organic afterglow nanoparticles with temperature and oxygen dual-responsive property for Bimodal sensing. *ACS Appl Nano Mater* 2023;6:15138–46. <https://doi.org/10.1021/acsnano.3c02770>.
- [11] Huang J, Deng X, Li J, Wang G, Li X, Yao H, et al. Developing robust organic afterglow emulsion for dissolved oxygen sensing. *Chem Eng J* 2023;474:145809. <https://doi.org/10.1016/j.cej.2023.145809>.
- [12] Li J, Wang G, Chen X, Li X, Wu M, Yuan S, et al. Manipulation of triplet excited states in two-component systems for high-performance organic afterglow materials. *Chem Eur J* 2022;28:e202200852. <https://doi.org/10.1002/chem.202200852>.
- [13] Forni A, Lucenti E, Botta C, Cariati E. Metal free room temperature phosphorescence from molecular self-interactions in the solid state. *J Mater Chem C* 2018;6:4603–26. <https://doi.org/10.1039/C8TC01007B>.
- [14] Yan X, Peng H, Xiang Y, Wang J, Yu L, Tao Y, et al. Recent advances on host–guest material systems toward organic room temperature phosphorescence. *Small* 2022;18:2104073. <https://doi.org/10.1002/smll.202104073>.
- [15] Gao H, Ma X. Recent progress on pure organic room temperature phosphorescent polymers. *Aggregate* 2021;2:e38. <https://doi.org/10.1002/agt.238>.
- [16] Zhang G, Palmer GM, Dewhurst MW, Fraser CL. A dual-emissive-materials design concept enables tumour hypoxia imaging. *Nat Mater* 2009;8:747–51. <https://doi.org/10.1038/nmat2509>.
- [17] Yuan WZ, Shen XY, Zhao H, Lam JWY, Tang L, Lu P, et al. Crystallization-induced phosphorescence of pure organic luminogens at room temperature. *J Phys Chem C* 2010;114:6090–9. <https://doi.org/10.1021/jp909388y>.
- [18] Bolton O, Lee K, Kim H-J, Lin KY, Kim J. Activating efficient phosphorescence from purely organic materials by crystal design. *Nat Chem* 2011;3:205–10. <https://doi.org/10.1038/nchem.984>.
- [19] Sun H, Zhu L. Achieving purely organic room temperature phosphorescence in aqueous solution. *Aggregate* 2023;4:e253. <https://doi.org/10.1002/agt.2253>.
- [20] Cai S, Yao X, Ma H, Shi H, An Z. Manipulating intermolecular interactions for ultralong organic phosphorescence. *Aggregate* 2023;4:e320. <https://doi.org/10.1002/agt.2320>.
- [21] Hirata S, Totani K, Zhang J, Yamashita T, Kaji H, Marder SR, et al. Efficient persistent room temperature phosphorescence in organic amorphous materials under ambient conditions. *Adv Funct Mater* 2013;23:3386–97. <https://doi.org/10.1002/adfm.201203706>.
- [22] Ning Y, Yang J, Si H, Wu H, Zheng X, Qin A, et al. Ultralong organic room-temperature phosphorescence of electron-donating and commercially available host and guest molecules through efficient Förster resonance energy transfer. *Sci China Chem* 2021;64:739–44. <https://doi.org/10.1007/s11426-020-9980-4>.
- [23] Kabe R, Notsuka N, Yoshida K, Adachi C. Afterglow organic light-emitting diode. *Adv Mater* 2016;28:655–60. <https://doi.org/10.1002/adma.201504321>.
- [24] Li Y, Gu F, Ding B, Zou L, Ma X. Photo-controllable room-temperature phosphorescence of organic photochromic polymers based on hexaarylbimidazole. *Sci China Chem* 2021;64:1297–301. <https://doi.org/10.1007/s11426-021-9978-1>.
- [25] Zhang X, Xie T, Cui M, Yang L, Sun X, Jiang J, et al. General design strategy for aromatic ketone-based single-component dual-emissive materials. *ACS Appl Mater Interfaces* 2014;6:2279–84. <https://doi.org/10.1021/am405209w>.
- [26] Zhai X, Zeng Y, Deng X, Lou Q, Cao A, Ji L, et al. Visible-light-excitible aqueous afterglow exhibiting long emission wavelength and ultralong afterglow lifetime of 7.64 s. *Chem Commun* 2023;59:10500–3. <https://doi.org/10.1039/D3CC03288D>.
- [27] Zhang K, Yeung MC-L, Leung SY-L, Yam VW-W. Manipulation of nanostructures in the co-assembly of platinum(II) complexes and block copolymers. *Chem* 2017;2:825–39. <https://doi.org/10.1016/j.chempr.2017.04.017>.
- [28] Zhang K, Yeung MC-L, Leung SY-L, Yam VW-W. Living supramolecular polymerization achieved by collaborative assembly of platinum(II) complexes and block copolymers. *Proc Natl Acad Sci USA* 2017;114:11844–9. <https://doi.org/10.1073/pnas.1712827114>.
- [29] Zhang K, Yeung MC-L, Leung SY-L, Yam VW-W. Energy landscape in supramolecular coassembly of platinum(II) complexes and polymers: morphological diversity, transformation, and dilution stability of nanostructures. *J Am Chem Soc* 2018;140:9594–605. <https://doi.org/10.1021/jacs.8b04779>.
- [30] Sun M-J, Liu Y, Yan Y, Li R, Shi Q, Zhao YS, et al. In situ visualization of assembly and photonic signal processing in a triplet light-harvesting nanosystem. *J Am Chem Soc* 2018;140:4269–78. <https://doi.org/10.1021/jacs.7b12519>.
- [31] Wan Q, To W-P, Chang X, Che C-M. Controlled synthesis of Pd^{II} and Pt^{II} supramolecular copolymer with sequential multiblock and amplified phosphorescence. *Chem* 2020;6:945–67. <https://doi.org/10.1016/j.chempr.2020.01.021>.
- [32] Hirata S, Totani K, Yamashita T, Adachi C, Vacha M. Large reverse saturable absorption under weak continuous incoherent light. *Nat Mater* 2014;13:938–46. <https://doi.org/10.1038/nmat4081>.
- [33] Bhattacharjee I, Hirata S. Highly efficient persistent room-temperature phosphorescence from heavy atom-free molecules triggered by hidden long phosphorescent antenna. *Adv Mater* 2020;32:2001348. <https://doi.org/10.1002/adma.202001348>.
- [34] Wang Y, Gao H, Yang J, Fang M, Ding D, Tang BZ, et al. High performance of simple organic phosphorescence host–guest materials and their application in time-resolved bioimaging. *Adv Mater* 2021;33:2007811. <https://doi.org/10.1002/adma.202007811>.
- [35] Zhou B, Wang G, Wang X, Guo W, Li J, Zhang K. Highly efficient room-temperature organic afterglow achieved by collaboration of luminescent dimeric TADF dopants and rigid matrices. *J Mater Chem C* 2021;9:3939–47. <https://doi.org/10.1039/d0tc05464j>.
- [36] Qian C, Ma Z, Fu X, Zhang X, Li Z, Jin H, et al. More than carbazole derivatives activate room temperature ultralong organic phosphorescence of benzoindole derivatives. *Adv Mater* 2022;34:2200544. <https://doi.org/10.1002/adma.202200544>.
- [37] Zhang X, Qian C, Ma Z, Fu X, Li Z, Jin H, et al. A class of organic units featuring matrix-controlled color-tunable ultralong organic room temperature phosphorescence. *Adv Sci* 2023;10:2206482. <https://doi.org/10.1002/advs.202206482>.
- [38] Qian C, Zhang X, Ma Z, Fu X, Li Z, Jin H, et al. Matrix-mediated color-tunable ultralong organic room temperature phosphorescence of 7-H-benzo[c]carbazole derivatives. *CCS Chem* 2023;1–14. <https://doi.org/10.31635/ccschem.023.202202561>.

- [39] Alam P, Leung NLC, Liu J, Cheung TS, Zhang X, He Z, et al. Two are better than one: a design principle for ultralong-persistent luminescence of pure organics. *Adv Mater* 2020;32:2001026. <https://doi.org/10.1002/adma.202001026>.
- [40] Wang X, Li J, Zeng Y, Chen X, Wu M, Wang G, et al. Merging thermally activated delayed fluorescence and two-photon ionization mechanisms for highly efficient and ultralong-lived organic afterglow. *Chem Eng J* 2023;460:141916. <https://doi.org/10.1016/j.cej.2023.141916>.
- [41] Jinnai K, Kabe R, Adachi C. Wide-range tuning and enhancement of organic long-persistent luminescence using emitter dopants. *Adv Mater* 2018;30:1800365. <https://doi.org/10.1002/adma.201800365>.
- [42] Liang X, Zheng Y, Zuo J. Two-Photon ionization induced stable white organic long-persistent luminescence. *Angew Chem Int Ed* 2021;60:16984–8. <https://doi.org/10.1002/anie.202106472>.
- [43] Li W, Li Z, Si C, Wong MY, Jinnai K, Gupta AK, et al. Organic long-persistent luminescence from a thermally activated delayed fluorescence compound. *Adv Mater* 2020;32:2003911. <https://doi.org/10.1002/adma.202003911>.
- [44] Xiao F, Gao H, Lei Y, Dai W, Liu M, Zheng X, et al. Guest-host doped strategy for constructing ultralong-lifetime near-infrared organic phosphorescence materials for bioimaging. *Nat Commun* 2022;13:186. <https://doi.org/10.1038/s41467-021-27914-0>.
- [45] Yang J, Wu X, Shi J, Tong B, Lei Y, Cai Z, et al. Achieving efficient phosphorescence and mechanoluminescence in organic host-guest system by energy transfer. *Adv Funct Mater* 2021;31:2108072. <https://doi.org/10.1002/adfm.202108072>.
- [46] Lei Y, Dai W, Guan J, Guo S, Ren F, Zhou Y, et al. Wide-range color-tunable organic phosphorescence materials for printable and writable security inks. *Angew Chem Int Ed* 2020;59:16054–60. <https://doi.org/10.1002/anie.202003585>.
- [47] Sun Y, Liu J, Li J, Li X, Wang X, Wang G, et al. Manipulation of triplet excited states for long-lived and efficient organic afterglow. *Adv Opt Mater* 2022;10:2101909. <https://doi.org/10.1002/adom.202101909>.
- [48] Wang X, Sun Y, Wang G, Li J, Li X, Zhang K. TADF-type organic afterglow. *Angew Chem Int Ed* 2021;60:17138–47. <https://doi.org/10.1002/anie.202105628>.
- [49] Wang X-F, Xiao H, Chen P-Z, Yang Q-Z, Chen B, Tung C-H, et al. Pure organic room temperature phosphorescence from excited dimers in self-assembled nanoparticles under visible and near-infrared irradiation in water. *J Am Chem Soc* 2019;141: 5045–50. <https://doi.org/10.1021/jacs.9b00859>.
- [50] Gillett AJ, Pershin A, Pandya R, Feldmann S, Sneyd AJ, Alvertis AM, et al. Dielectric control of reverse intersystem crossing in thermally activated delayed fluorescence emitters. *Nat Mater* 2022;21:1150–7. <https://doi.org/10.1038/s41563-022-01321-2>.
- [51] Samanta PK, Kim D, Coropceanu V, Brédas J-L. Up-conversion intersystem crossing rates in organic emitters for thermally activated delayed fluorescence: impact of the nature of singlet vs triplet excited states. *J Am Chem Soc* 2017;139:4042–51. <https://doi.org/10.1021/jacs.6b12124>.
- [52] Lee K, Kim D. Local-excitation versus charge-transfer characters in the triplet state: theoretical insight into the singlet-triplet energy differences of carbazolyl-phthalonitrile-based thermally activated delayed fluorescence materials. *J Phys Chem C* 2016;120:28330–6. <https://doi.org/10.1021/acs.jpcc.6b10161>.
- [53] Sun Y, Liu J, Li J, Li X, Wang X, Wang G, et al. Manipulation of triplet excited states for long-lived and efficient organic afterglow. *Adv Opt Mater* 2022;10:2101909. <https://doi.org/10.1002/adom.202101909>.
- [54] Wang X, Sun Y, Wang G, Li J, Li X, Zhang K. TADF-type organic afterglow. *Angew Chem Int Ed* 2021;60:17138–47. <https://doi.org/10.1002/anie.202105628>.
- [55] Su Y, Wu M, Wang G, Li J, Chen X, Li X, et al. Benzophenone-containing phosphors with an unprecedented long lifetime of 1.8 s under ambient conditions. *Chem Commun* 2023;59:1525–8. <https://doi.org/10.1039/D2CC06601G>.
- [56] Ding S, Xu Y, Li J, Wang X, Wang G, Li H, et al. Achieving long-lived room-temperature phosphorescence via charge transfer technology and dopant-matrix design strategy. *Dyes Pigments* 2023;210:110984. <https://doi.org/10.1016/j.dyepig.2022.110984>.
- [57] Chen X, Wang G, Li J, Chen X, Zhao X, Zeng Y, et al. Difluoroboron β -diketonate systems: large transformation of photophysical mechanism induced by tiny structural modification or isomerization. *Adv Opt Mater* 2023;2301619. <https://doi.org/10.1002/adom.202301619>.
- [58] El-Sayed MA. The triplet state: its radiative and nonradiative properties. *Acc Chem Res* 1968;1:8–16. <https://doi.org/10.1021/ar50001a002>.
- [59] Wu M, Wang X, Pan Y, Li J, Li X, Sun Y, et al. Two-component design strategy: achieving intense organic afterglow and diverse functions in coronene-matrix systems. *J Phys Chem C* 2021;125:26986–98. <https://doi.org/10.1021/acs.jpcc.1c08409>.
- [60] Li J, Wang X, Zhao X, Chen X, Ding S, Wu M, et al. Cascade synthesis of luminescent difluoroboron diketonate compounds for room-temperature organic afterglow materials. *Chin J Chem* 2022;40:2507–15. <https://doi.org/10.1002/cjoc.202200354>.
- [61] Li J, Wang X, Pan Y, Sun Y, Wang G, Zhang K. Unexpected long room-temperature phosphorescence lifetimes of up to 1.0 s observed in iodinated molecular systems. *Chem Commun* 2021;57:8794–7. <https://doi.org/10.1039/diccc04094d>.
- [62] Frisch MJ, Trucks GW, Schlegel HB, Scuseria GE, Robb MA, Cheeseman JR, et al. *Gaussian 16 Rev. A.03*. 2016.
- [63] Becke AD. Density-functional exchange-energy approximation with correct asymptotic behavior. *Phys Rev* 1988;38:3098–100. <https://doi.org/10.1103/PhysRevA.38.3098>.
- [64] Lee C, Yang W, Parr RG. Development of the colle-salvetti correlation-energy formula into a functional of the electron density. *Phys Rev B* 1988;37:785–9. <https://doi.org/10.1103/PhysRevB.37.785>.
- [65] Neese F. Software update: the ORCA program system—version 5.0. *WIREs Comput Mol Sci* 2022;12:e1606. <https://doi.org/10.1002/wcms.1606>.
- [66] Lu T, Chen F. Multiwfn: a multifunctional wavefunction analyzer. *J Comput Chem* 2012;33:580–92. <https://doi.org/10.1002/jcc.22885>.
- [67] Liu Z, Lu T, Chen Q. An sp-hybridized all-carbon atom ring, cyclo[18]carbon: electronic structure, electronic spectrum, and optical nonlinearity. *Carbon* 2020; 165:461–7. <https://doi.org/10.1016/j.carbon.2020.05.023>.
- [68] Humphrey W, Dalke A, Schulten K. VMD: Visual molecular dynamics. *J Mol Graph* 1996;14:33–8. [https://doi.org/10.1016/0263-7855\(96\)00018-5](https://doi.org/10.1016/0263-7855(96)00018-5).
- [69] Martin RL. Natural transition orbitals. *J Chem Phys* 2003;118:4775–7. <https://doi.org/10.1063/1.1558471>.
- [70] Zeng Y, Zhai X, Wang G, Su Y, Wu M, Wang B, et al. Transformation of organic afterglow mechanism from room-temperature phosphorescence to thermally-activated delayed fluorescence in intramolecular charge transfer systems. *Dyes Pigments* 2023;219:111643. <https://doi.org/10.1016/j.dyepig.2023.111643>.
- [71] Li J, Li X, Wang G, Wang X, Wu M, Liu J, et al. A direct observation of up-converted room-temperature phosphorescence in an anti-Kasha dopant-matrix system. *Nat Commun* 2023;14:1987. <https://doi.org/10.1038/s41467-023-37662-y>.
- [72] Liu J, Sun Y, Wang G, Chen X, Li J, Wang X, et al. Organic afterglow emulsions exhibiting 2.4 s phosphorescence lifetimes and specific protein binding property. *Adv Opt Mater* 2022;2201502. <https://doi.org/10.1002/adom.202201502>.
- [73] Li X, Wang G, Li J, Sun Y, Deng X, Zhang K. Intense organic afterglow enabled by molecular engineering in dopant-matrix systems. *ACS Appl Mater Interfaces* 2022; 14:1587–600. <https://doi.org/10.1021/acsami.1c20331>.